INT. J. REMOTE SENSING, 2002, VOL. 23, NO. 8, 1733–1739

Texture based feature extraction: application to burn scar detection in Earth observation satellite sensor imagery

A. M. S. SMITH†, M. J. WOOSTER†, A. K. POWELL‡ and D. USHER‡

†Department of Geography, Kings College London, London, England, UK, WC2R 2LS; e-mail: alistair_smith_kcl@yahoo.co.uk; martin.wooster@kcl.ac.uk
‡Department of Physics, Kings College London, London, England, UK, WC2R 2LS; e-mail: kp@maxwell.ph.kcl.ac.uk; david.usher@kcl.ac.uk,

(*Received 4 January 2001; in final form 19 October 2001*)

Abstract. A single band texture-based burn scar identification algorithm incorporating the use of grey level co-occurrence matrices with a low pass filtering technique is described and demonstrated using 1km resolution ATSR-2 imagery of burned savannas in southern Sudan. The algorithm results are compared to those produced by the iterative intensity-based isodata classification technique. The accuracy of each of these methods was evaluated by comparison with 18 m spatial resolution imagery. For a set of 22 sample fire scars of varying area Pearson correlation coefficients of 0.75 and 0.94 were obtained between the burnt area statistics produced with the low-spatial resolution texture and isodata methods respectively and those produced using the high-resolution data. The classification quality, as described by the Kappa (k) statistic, produced values of $k_{\mathrm{TEXTURE}} = 0.558$ and $k_{\mathrm{ISODATA}} = 0.852$. Texture is shown to be an image variable capable of highlighting burned area in low spatial resolution imagery, but the currently tested approach offers no accuracy of quality benefit over the solely intensity-based method.

1. Introduction

Previous image processing studies have used grey level co-occurrence matrices (GLCMs) within texture-based feature classification algorithms. Researchers in medical imaging have used GLCMs to identify the cataract symptoms in retinal scans (Paplinski and Boyce 1997) whilst in recent years the Earth observation (EO) community have used GLCMs in urban land use classification (Karathanassi *et al.* 2000).

The current study aimed to investigate the potential of texture-based GLCM techniques for the identification of burn scars in low spatial resolution EO imagery since most current burn scar mapping techniques rely solely on pixel intensity information. The main focus of attention for texture-based classification in EO has been in determining the internal pixel structure of image regions since in general these methods fail to detect convoluted edges and small isolated features (Warner 1999).

Accurate estimates of the area burned by fire are important in natural hazard applications and in calculating the resultant gas and aerosol emissions. In tropical savanna environments, 80–100% of the vegetation is combusted in the largest fires that

International Journal of Remote Sensing
ISSN 0143-1161 print/ISSN 1366-5901 online © 2002 Taylor & Francis Ltd
http://www.tandf.co.uk/journals
DOI: 10.1080/01431160110106104

can each affect hundreds or thousands of square kilometres (Eva and Lambin 1998). In such environments fire scar detection algorithms can rely on low spatial resolution imagery since isolated small patches of burned area are relatively unimportant.

2. Data and pre-processing

Three daytime 512 km × 512 km ATSR-2 scenes of a savanna region in southern Sudan were used for this test case (10, 13 and 17 December 1995). Previous studies have shown that the near-infrared spectral region is particularly effective for detecting burned area (Trigg and Flasse 2000), so the ATSR-2 0.87 μm channel was used in this study. Due to data rate limitations on the ERS-2 satellite, continental (i.e. non-oceanic) imagery from the ATSR-2 optical wavebands (0.55, 0.67, 0.87 and 1.6 μm) is sometimes available in only a subset of channels. Furthermore the mid-infrared channel (3.7 μm) is frequently saturated over hot savanna regions. In such cases, a texture-based algorithm that could operate on only a single waveband of data may be a useful tool. The 0.87 μm data were pre-processed to mask water features to reduce computational cost and were converted into surface reflectance using standard conversion tables[1].

Comparison data for accuracy assessment were provided by a 100 km × 100 km spatial resolution of 18 m Optical Sensor (OPS) image of the region, taken on 20 December 1995 and shown in figure 1. Active fires were easily identified in the OPS imagery due to their visible smoke plumes. Active fires were rare in the areas chosen for accuracy assessment, allowing us to assume that the OPS and ATSR-2 scenes depicted very similar ground situations. The matching OPS and ATSR sub-scenes were geo-coded to latitude/longitude grids with pixel sizes equivalent to 18 m (OPS) and 1 km (ATSR) respectively. The texture based (GLCM) and intensity based (isodata) classification methods were applied to the ATSR-2 data, with results compared to an independent classification of the OPS imagery that we assume here shows the 'true' situation.

3. Background

3.1. *Grey level co-occurrence matrices*

The GLCM is produced by the application of an operator to the original image data. A simple case, illustrated in column A of figure 2 (Process 1), demonstrates that the instances when the output from the two halves of the kernel are equal ($x = y$) will be recorded on the GLCM centre diagonal and when $x \neq y$ these instances will be recorded in the off-diagonal locations. Thus the centre diagonal contains the class region information whilst the off-diagonal areas contain class boundary information.

In medical imaging some of the most accurate texture-based classifiers have been implemented using bow-tie operators, as seen in the model implementation (column B) of figure 2, since these enhance the textural properties of the pixel groups (Paplinski and Boyce 1997). These operators define x and y as being the variance of the weighted values in the left-hand and right-hand side of the operator respectively. The variance is chosen since the texture of a given feature can be recognised as being a variation in the grey level contrast, or intensity, over a finite sample space (Titterington *et al.* 1985).

[1] The conversion tables can be found at the Rutherford Appleton Laboratory website at http://www.atsr.rl.ac.uk

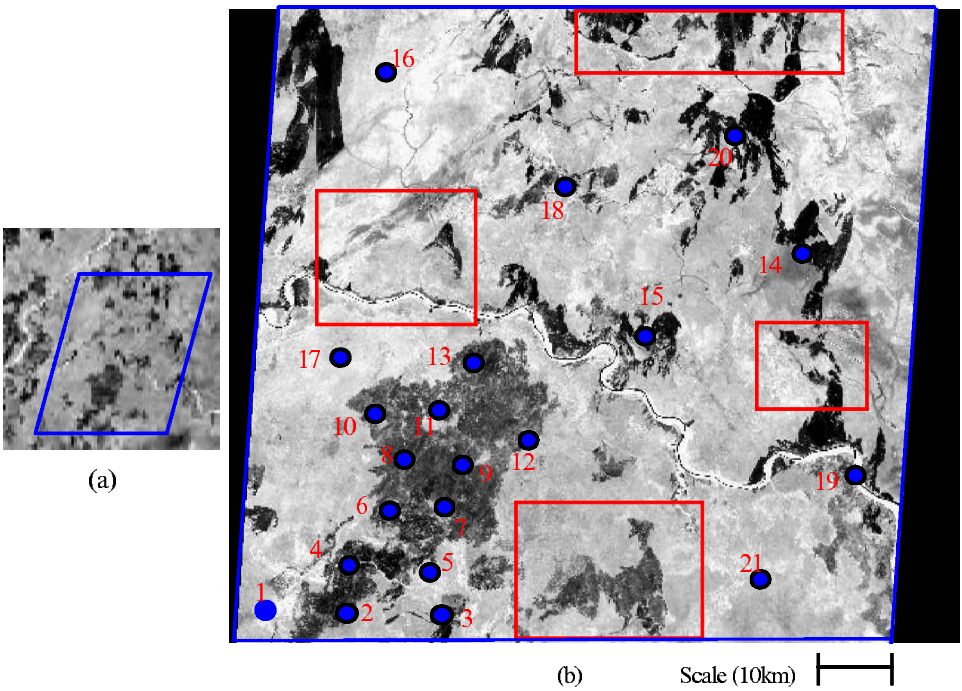

Figure 1. Southern Sudanian savanna containing burned areas (dark patches) with centre Latitude 8.3°, Longitude 32.1°. (a) 150 km × 150 km ATSR-2 0.87 μm scene segment. The blue border marks the extent of the OPS scene. (b) OPS 0.76 μm scene: Blue dots—centre points of segments used in accuracy assessment, Red rectangles—excluded areas due to active fires.

3.2. *The isodata classification algorithm*

Isodata is an automated intensity-based classifier, with the approximate number of classes predetermined by the user (typically 5–10). The algorithm initially estimates the mean positions of each of the evenly distributed intensity classes within the original image histogram. The remaining pixels are then iteratively clustered using a minimum distance classifier. On each iteration the class means are recalculated and the pixels reclassified, this continuing until the number of pixels in each class changes by less than a set threshold or the maximum number of iterations is reached (Ball and Hall 1965).

4. Method

The bow-tie operator shown in figure 2 (Process 1) was convolved with each of the ATSR-2 0.87 μm scenes to produce a co-occurrence matrix. The projection of the GLCM's centre diagonal produced a distribution that contained the incidence information of the different texture groups. Each bin of this effective 'texture histogram' corresponds to a (x = bin number, y = bin number) co-ordinate on the GLCM centre diagonal. The main texture classes can be obtained by identifying the principal maxima of this histogram (Paplinski and Boyce 1997). As seen in figure 2 (Process 2), a low pass filtering technique was used to remove the high frequency class boundaries and isolate the prominent histogram maxima (less than 30).

Applying a minimum distance classifier to each x and y pair obtained from the GLCM process achieved the classification.

Intensity-based classification of the same scene was achieved through use of the isodata classification technique with a threshold of seven classes. The GLCM texture and isodata intensity classes corresponding to burn scars were identified by visual examination in order to produce the final classified burn scar data sets.

5. Accuracy assessment

Comparison data for accuracy assessment were derived from burn scar maps produced from the OPS high spatial resolution imagery classified using isodata optimised by visual inspection. The classification accuracy of the ATSR-2 methods was determined using an established approach to compare coincident areas from the classified high and low spatial resolution data sets (Eva and Lambin 1998).

The areas burned within twenty-two randomly located 9 km × 9 km sample sites selected in the spatially co-incident ATSR-2 and OPS data (represented by blue dots in figure 1) were compared through use of Pearson correlation coefficients. Measures of the classification accuracy were achieved using the Kappa (KHAT) statistic (Karathanassi *et al.* 2000) from 11 random sets of 400 pixels from within the test region.

6. Results

The test criteria for the classification methods are:

1. For R^2: >0.700 practically applicable classification method
   <0.700 poor classification method. (Fuller and Fulk 2001)
2. For k: >0.8 strong agreement
   0.4–0.8 moderate agreement
   <0.4 poor agreement (Landis and Kock 1977)

6.1. *Area accuracy assessment*

Figure 3(a) presents the percentage area burned within each sample site using each classification method applied to ATSR-2, compared to the high spatial resolution classification. The texture-based method tends to under-estimate area burned, as is indicated by the 0.8:1 line of best fit. The R^2 value between these data and those from the OPS scene is 0.72. The isodata method applied to ATSR-2 produced a more accurate result, as seen by the majority of the sample points lying around the 1:1 line in figure 3(a) and by the R^2 value of 0.95.

Figure 2. Process 1—The operator is convolved with the image and the incidence of each possible (x, y) pair is recorded within the GLCM. The red line indicates the central diagonal on which the main texture regions are identified. Different colours denote which pixels lie within each class. The positions of each texture class peak (red column) are used in Process 2. Process 2—The upper row histogram represents the planar projection of the GLCM's centre diagonal. The bar chart shows the locations of the histogram maxima. As seen in the process column the values of the adjacent histogram bins (the numbers represent the actual bin numbers) are summed, resulting in a new histogram (lower row) with bin numbers exactly half those of the original and thus having effectively half the resolution. This process is repeated until peaks <30. The peak positions are then mapped back to the equivalent $(x = y)$ positions on the centre diagonal of the GLCM.

PROCESS 1

Column A:
ILLUSTRATION

Simple Bow-tie operator

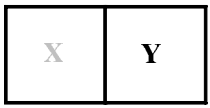

Column B:
IMPLEMENTED CASE

Implemented Bow-tie operator

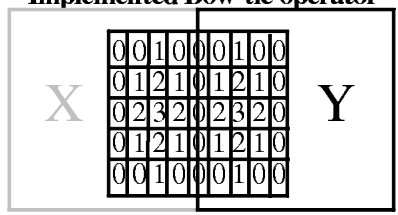

KERNEL

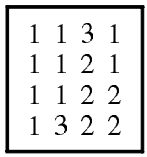

IMAGE

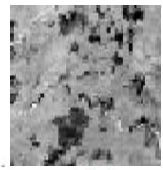

GLCM

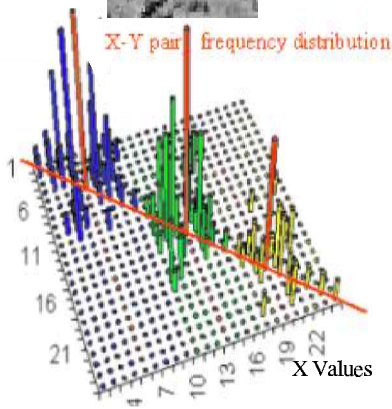

$C(1,1) = 3 \quad C(1,2) = 2 \quad C(1,2) = 2$

$C(2,1) = 1 \quad C(2,2) = 2 \quad C(2,3) = 0$

$C(3,1) = 1 \quad C(3,2) = 1 \quad C(3,3) = 0$

PROCESS 2

PROCESS

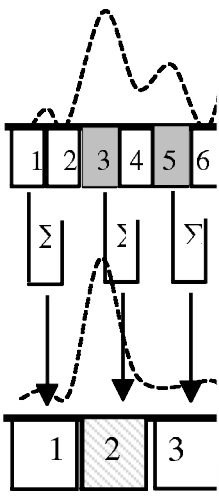

HISTOGRAMS

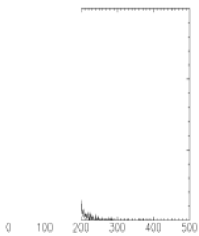

Initial Output

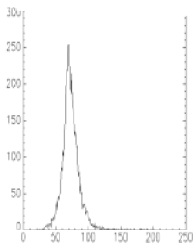

Subsequent Output

BAR CHARTS

Original res, histogram maximum positions

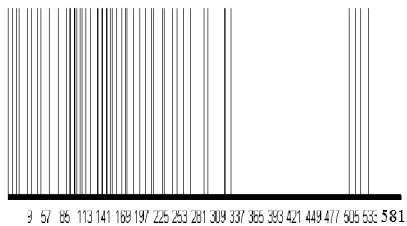

Half res, histogram maximum positions

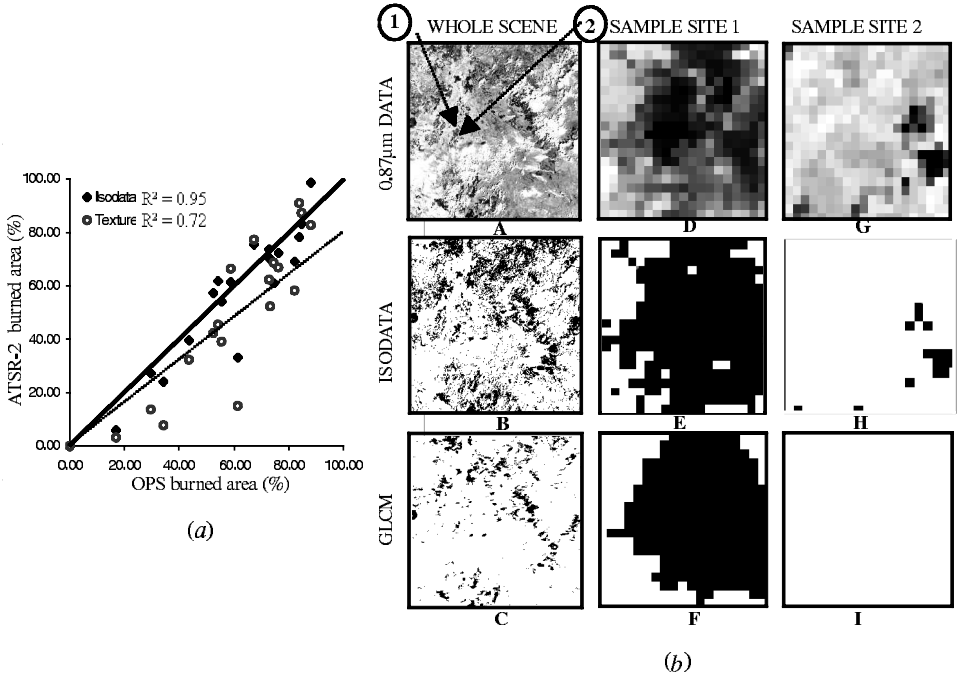

Figure 3. (*a*) Comparison of ATSR-2 isodata and texture classifications to the OPS imagery. The solid line indicates a 1:1 relationship whilst the dashed line indicates 1:0.8. (*b*) ATSR-2 data and derived isodata and texture classifications, with sample sites 1 and 2 highlighted on the whole scene image.

6.2. *Area quality assessment*

Inspection of the images reveals the GLCM algorithm's relative inability to detect small (single-pixel) areas and the edges of the larger scars. However, it accurately identifies the central regions of large burned areas. This result is an inherent limitation of using only information derived from the centre diagonal of the GLCM since this automatically discards potentially useful information for identifying the class borders.

Figure 3(b) illustrates the two possible extremes. At Sample Site 1, a large percentage of pixels are burned as identified by the predominance of dark pixels in D. E demonstrates the isodata algorithm's low errors of omission, whilst F shows that the texture approach often fails to detect the burn scar edge pixels but does identify the main burned area. At Sample Site 2 the percentage of burned pixels is low (G), whilst H and I show that both low spatial resolution techniques have low errors of commission but that the texture method fails to identify the few isolated burned pixels. These observations are borne out by the Kappa values of $k_{\mathrm{TEXTURE}} = 0.558$ and $k_{\mathrm{ISODATA}} = 0.852$ obtained from the 11×400 pixel set analysis.

7. Conclusions

With respect to the test criterion, the texture-based GLCM classifier satisfied the first test and achieved a moderate agreement for the second, whilst the intensity-based isodata classifier satisfied the first test and produced a strong agreement for the second. In conclusion, texture appears to be an image variable that can be used to identify burn scars in EO data. However, using the present GLCM centre diagonal

projection does not produce any benefits over the solely intensity-based isodata algorithm. Approaches in the medical imaging community are now being developed that use the complete 2-dimensional GLCM and that may prove more beneficial in classifying both central and border regions.

References

Ball, G. H., and Hall, D. J., 1965, ISODATA, a novel method of data analysis and pattern classification. Technical Report, Stanford Research Institute, Melo Park, California, USA.

Eva, H., and Lambin, E. F., 1998, Burnt area mapping in central Africa using ATSR data. *International Journal of Remote Sensing*, **19**, 3473–3497.

Fuller, D. O., and Fulk, M., 2001, Burned area in Kalimantan, Indonesia mapped with NOAA-AVHRR and Landsat TM imagery. *International Journal of Remote Sensing*, **22**, 691–698.

Karathanassi, V., Iossifidis, C. H., and Rokos, D., 2000, A texture-based classification method for classifying built areas according to their density. *International Journal of Remote Sensing*, **21**, 1807–1823.

Landis, J. R., and Kock, G. G., 1977, The measurement of observer agreement for categorical data. *Biometrics*, **33**, 159–174.

Paplinski, A. P., and Boyce, J. F., 1997, Segmentation of a class of ophthalmological images using a directional variance operator and co-occurrence arrays. *Optical Engineering*, **36**, 3140–3147.

Titterington, D. M., Smith, A. F. M., and Makov, U. E., 1985, *Statistical analysis of finite mixture distributions* (Chichester: Wiley).

Trigg, S., and Flasse, S., 2000, Characterising the spectral-temporal response of burned savannah using in situ spectroradiometry and infrared thermometry. *International Journal of Remote Sensing*, **21**, 3161–3168.

Warner, T. A., 1999, Analysis of spatial patterns in remotely sensed data using multivariate spatial correlation. *Geocarto International*, **14**, 1.